frontiers in Astronomy and Space Sciences

REVIEW
published: 04 January 2022
doi: 10.3389/fspas.2021.745357

A Review of Observations of Molecular Ions in the Earth's Magnetosphere-Ionosphere System

Mei-Yun Lin and Raluca Ilie*

Department of Electrical and Computer Engineering, University of Illinois at Urbana-Champaign, Urbana, IL, United States

Ionospheric molecular ions, such as NO^+, N_2^+ and O_2^+, are gravitationally bound, and are expected to undergo recombination to form a pair of neutral atoms, due to short dissociative recombination lifetime. Therefore, they are expected to be relatively cold in the Earth's atmosphere, compared with light ions such as H^+ and He^+, or even heavier ions such as N^+ or O^+. However, several spacecraft missions observed their presence in the high-altitude ionosphere and the magnetosphere, predominantly during the geomagnetically active times. This hints to the possibility that molecular ions have the ability to acquire sufficient energy in a very short time, and can be used as tracers of mass differentiated vertical transport to understand the mechanisms responsible for "fast ionospheric outflow." In this letter, we review the observational data sets that reported on the abundances of molecular ions in the Earth's magnetosphere-ionosphere system, starting from their first observations by the Sputnik III mission, to the current Arase (ERG) satellite and Enhanced Polar Outflow Probe (e-POP) missions. The available data suggests that molecular ions are quite abundant in the lower atmosphere at all times, but are only seen in the high-altitude ionosphere and magnetosphere during the times of increased geomagnetic activity.

Keywords: ionospheric outflow, molecular ions, cold plasma, heavy ions, polar wind

OPEN ACCESS

Edited by:
Gian Luca Delzanno, Los Alamos National Laboratory (DOE), United States

Reviewed by:
Katherine Garcia-Sage, National Aeronautics and Space Administration, United States
Roger Varney, SRI International, United States

****Correspondence:***
Mei-Yun Lin
mylin2@illinois.edu

Specialty section:
This article was submitted to Space Physics, a section of the journal Frontiers in Astronomy and Space Sciences

Received: *21 July 2021*
Accepted: *22 November 2021*
Published: *04 January 2022*

Citation:
Lin M-Y and Ilie R (2022) A Review of Observations of Molecular Ions in the Earth's Magnetosphere-Ionosphere System. Front. Astron. Space Sci. 8:745357. doi: 10.3389/fspas.2021.745357

1 INTRODUCTION

Singly charged heavy ions observed in the magnetosphere, such as atomic N^+ and O^+, and molecular N_2^+, NO^+, and O_2^+ ions, are sourced from the Earth's ionosphere, and transported outward through the process of ionospheric escape. One of the main pathways of ionospheric loss is the polar wind, an ambipolar flow of plasma from the high-latitude ionosphere to the low pressure magnetosphere. This outflow (Axford and Hines, 1961; Shelley et al., 1972; Yau et al., 1991; Maggiolo et al., 2006; Schunk and Nagy, 2009; Kronberg et al., 2014; Ilie and Liemohn, 2016; Glocer et al., 2018; Lin et al., 2020) provides a pathway for atmospheric migration and escape at a rate that generally depends on solar extreme ultraviolet (EUV) photon flux striking the upper atmosphere, as well the electromagnetic driving from the solar wind. Therefore, heavy ions of ionospheric origin can be directed and further circulated into different regions of the magnetosphere: either on closed magnetic field lines (plasma sheet) where ions can potentially be returned to the ionosphere, or on open magnetic field lines (lobe region) directly connected to the interplanetary magnetic field where ions are lost to space (Christon et al., 1994; Haaland et al., 2012a; Haaland et al., 2012b; Ilie et al., 2013; Yamauchi, 2019). **Figure 1** shows an illustration of polar wind ion species, which could be created by the photoionization with the neutral atmosphere (and other ion-neutral-electron chemical reactions) and accelerated along magnetic field lines.

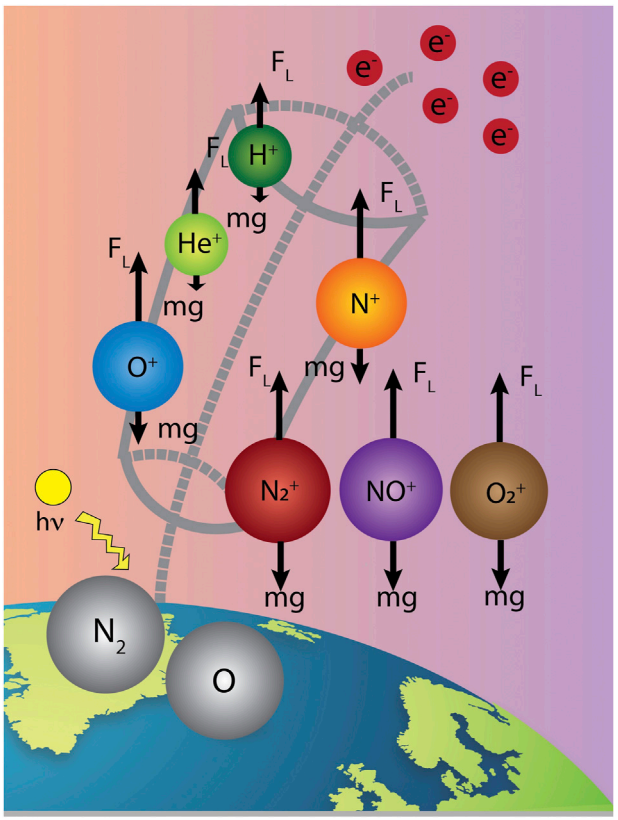

FIGURE 1 | Diagram of relevant ionospheric species (H^+, He^+,O^+, N^+, N_2^+, NO^+ and O_2^+) and electrons (e^-), with the forces they experience through the vertical transport: gravity (mg) and electromagnetic force (F_L). Following the open magnetic field line (grey dashed line), the polar wind plasma transports along the magnetic flux tube (grey cone around the dashed grey line). This illustration shows only O and N_2 species only, although the neutral composition at low altitudes includes additional species (as discussed in **Section 4**).

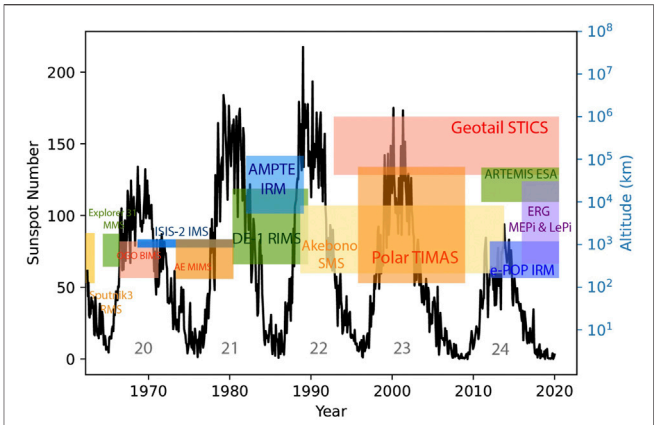

FIGURE 2 | Sunspot number from 1958 to 2021 (black lines) indicative of solar cycles 19 through 24 (numbers in grey). Over-plotted are the missions that reported on observations of molecular ions and their corresponding operating region in space, along with the timeframe of operation. Note that in most cases the actual data availability covers a time window less than the mission lifetime.

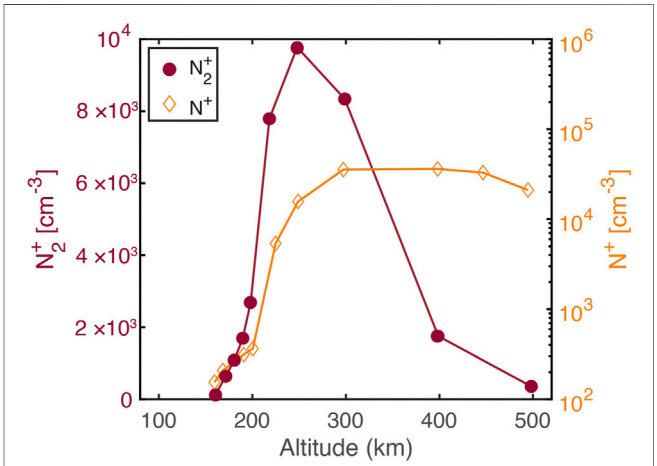

FIGURE 3 | First direct ions densities measurements by the Soviet Sputnik III satellite with the altitude profile (*x*-axis) for molecular N_2^+ (magenta line) and atomic N^+ ions (orange line) in the upper atmosphere. Noted that the left y-axis (N_2^+ ions density) and right y-axis (N^+ ions density) are on different scales. Figure digitized and adapted from (Istomin, 1966).

The dynamics leading to the ionospheric outflow of O^+ ions, and the impact on the evolution of the Earth's magnetosphere-ionosphere system have been the subject of numerous studies (e.g., Schunk and Raitt, 1980; Mukai et al., 1994; Schunk and Sojka, 1997; Seki et al., 1998; Daglis et al., 1999; Moore et al., 1999; Winglee et al., 2002; Nosé et al., 2005; Barakat and Schunk, 2006; Yau et al., 2007; Glocer et al., 2009; Garcia et al., 2010; Glocer et al., 2012; Ilie et al., 2013; Ilie et al., 2015; Lin et al., 2020). In contrast, the transport and energization of molecular ions, in addition to that of N^+ and O^+ ions, have received less attention, most likely due to the scarcity of measurements.

It is known that N_2^+, NO^+, and O_2^+ ions are the major ion populations in the ionospheric E and F layers, and primarily created through photoionization and ion-neutral-electron chemical reactions. These molecular ions maintain low energies due to their large masses and short dissociative recombination lifetimes with electrons, as they quickly form a pair of neutral atoms. In the F layer, the reaction rates of dissociative recombination of O_2^+ and NO^+ are approximately $10^{-7}\,cm^{-3}\,s^{-1}$, while those of the charge exchange reactions to remove O^+ are approximately $10^{-11}\,cm^{-3}\,s^{-1}$. Despite the fact that the abundance of molecular ions decreases significantly in the F2 layer, multiple missions reported their presence throughout the magnetosphere-ionosphere system (Taylor, 1974; Grebowsky et al., 1983; Craven et al., 1985; Klecker et al., 1986; Yau et al., 1993; Christon et al., 1994; Wilson and Craven, 1999; Lennartsson et al., 2000; Seki et al., 2019; Christon et al., 2020).

Figure 2 shows space missions that reported observations of molecular ions, starting from the early Sputnik III spacecraft to the Arase (ERG) mission, spanning from few hundreds km altitude to hundreds of Earth radii across several solar cycles. In this letter, we review the observational record of molecular ions from the Earth's terrestrial high latitude ionosphere to the magnetosphere. These observations provide context to understand the energization of

molecular ions, as well as to help interpret plasma observations from current and past space missions.

2 OBSERVATIONS OF MOLECULAR IONS IN THE IONOSPHERE

Molecular N_2^+ ions were first observed in the topside ionosphere by the Bennett-type radio frequency (RF) quadrupole mass spectrometer on board of the Soviet Sputnik III satellite (Nauk and Doklady, 1961). Launched on May 15, 1958, Sputnik III satellite aimed to observe the ionic compositions in the topside ionosphere, and its altitude range covered from 217 to 1864 km with 65.18° orbital inclination. **Figure 3** presents the first *in situ* observations of N^+ and N_2^+ densities as a function of altitude. These measurements from Sputnik III show that the density of N_2^+ is higher than that of N^+ at altitudes below 300 km, reaching a peak density of 9.8×10^3 cm^{-3} around 250 km altitude (Istomin, 1966). The reason for the fast decrease in N_2^+ density at higher altitudes is that in the F2 layer, N_2^+ undergoes fast recombination reactions with electrons to form a pair of neutral atoms, and charge exchanges quickly with most of the other neutral species. Thus, the concentration of N_2^+ rapidly decreases above 300 km altitude. On the other hand, N^+ is produced via N_2^+ dissociation and its concentration increases rapidly by 2–3 orders of magnitude as the altitude increases.

Previous observational data sets (Taylor et al., 1968; Johnson and Gerardo, 1972; Taylor, 1973) indicated that the abundances of molecular ions rapidly decreased due to short dissociative recombination lifetime, and therefore molecular ions were only occasionally observed. Thus, it has been concluded that the density of molecular ions in the topsides ionosphere is negligible. However, the Polar Orbiting Geophysical Observatory (OGO 6) mission launched on June 5, 1969, one of the first U.S. led large observatory to study the dynamics of high-altitude atmospheric parameters (Jackson and Vette, 1975), was the first to report observations of the high latitude trough (HLT), a prominent feature associated with the presence of molecular ions in the topside ionosphere (600–1,000 km). This HLT is a narrow (6°–10° latitude) region where the concentration of atomic H^+, He^+, O^+ and N^+ were observed to decrease by a factor of 3 or more, while molecular N_2^+, NO^+, and O_2^+ ion densities presented abrupt enhancements.

Although the inclination of the OGO 6 orbit was 82° north, due to the tilt of the dipole axis, OGO 6 covered a wide range of latitudes (Taylor, 1971), and the data coverage ranges from ~ 413 km to ~ 1077 km altitude. These unexpectedly abrupt and pronounced distributions of molecular ions were measured by the Bennett-type radio frequency ion mass spectrometer (Taylor, 1973) onboard OGO 6, showing enhancements in the density of NO^+ that reached 10^3 cm^{-3} at 1,000 km altitude near 70°–80° latitude, both in the northern and southern hemisphere, during the modest storm of June 20, 1970 (Max Kp = 4; Min Dst = −54 nT).

These large gradients in the abundances of molecular ions observed in the HLTs were later explained by the enhancement of soft electron precipitation associated with the polar cap region and the rapid loss of O^+ due to the strong electric

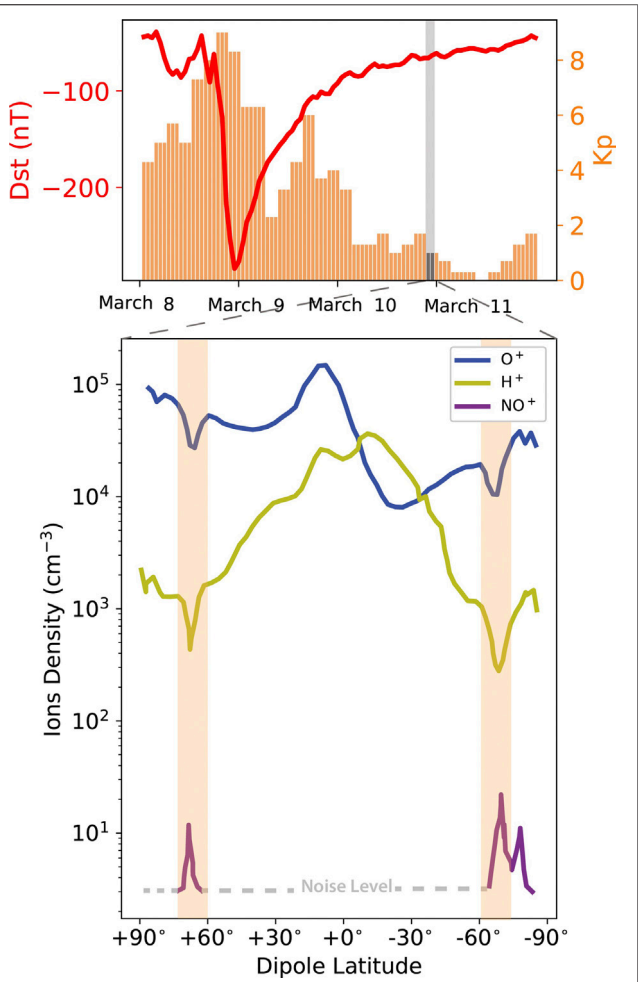

FIGURE 4 | Bottom panel shows the observed ion compositions of O^+ (blue), H^+ (light green) and NO^+ (purple) from OGO 6 satellite versus the latitudes, extracted during the recovery phase of March 8, 1970 geomagnetic storm. Note that the light orange blocks highlighted the HLTs with abrupt enhancements of NO^+ densities and decreases of atomic O^+ and H^+ ions densities. The Kp (orange bars) and Dst (red) indices during this storm are provided for reference. Figure digitized and adapted from (Taylor et al., 1975), and dipole latitudes in the *x*-axis are also identified as geomagnetic latitudes.

convection field (Taylor et al., 1975; Grebowsky et al., 1976; Grebowsky et al., 1983). On March 10, 1970, 1 day after the intense geomagnetic storm of March 8, 1970 (Max Kp = 9; Min Dst = -285 nT), the HLT was observed at altitudes between 700–800 km, and ~ 65.8° latitude in the northern hemisphere and ~ -65.2° latitude in the southern hemisphere. **Figure 4** shows the measurements of O^+, H^+ and NO^+ densities from OGO 6 satellite versus latitudes, extracted during the recovery phase of March 8, 1970 geomagnetic storm. It can be seen that in both HLT regions (with ~ 5° latitude range, highlighted as light orange), ~ 50% of both O^+ and H^+ densities are depleted at a time when NO^+ ions density increased about a factor of 8, while the peak value of NO^+ concentration was up to 20 cm^{-3} at ~ 700 km altitude. These observations suggest that the rapid loss of O^+ in the HLTs could contribute to the source of NO^+

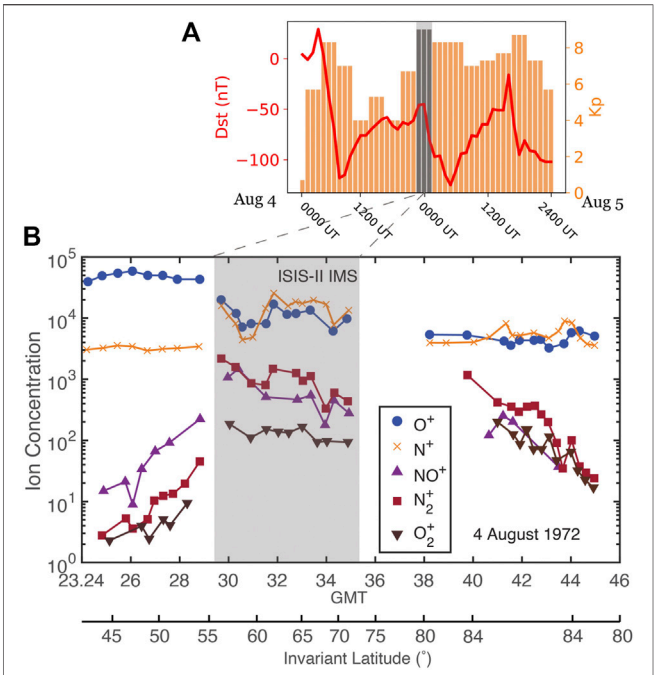

FIGURE 5 | High latitude ISIS 2 measurements showing the ion compositions of O^+ (blue), N^+ (orange), NO^+ (purple), N_2^+ (magenta) and O_2^+ (black), at 1,400 km altitude **(B)** during the storm of August 4, 1972. The measurements were observed along the ISIS 2 satellite trajectory, which is shown here as the combination of Greenwich Mean Time (GMT) and invariant latitudes. The Kp (orange bars) and Dst (red line) indices during this storm are shown for reference **(A)**; greyed out area on top panel corresponds to the time interval when the measurements present in bottom panel are extracted. Figure digitized and adapted from (Hoffman et al., 1974).

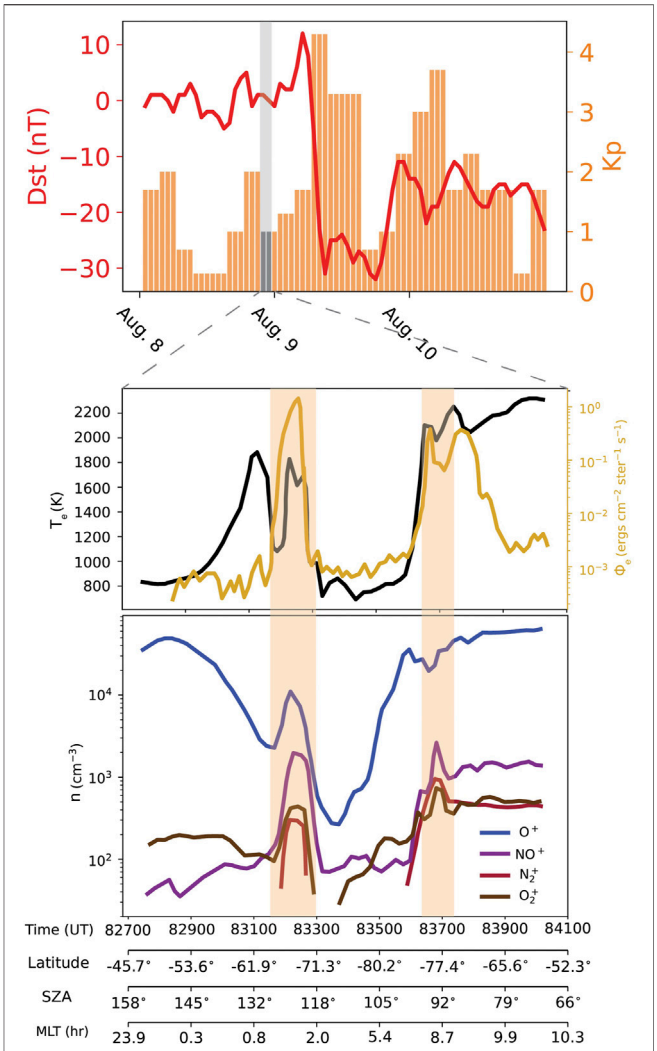

FIGURE 6 | AE-C measurement during the winter solar minimum at high southern latitude F layer. The bottom panel shows the ion compositions (n) of O^+ (blue line), NO^+ (purple line), N_2^+ (magenta line) and O_2^+ (black line) when the AE-C passed the orbit of 14 182 (versus UT, latitude and MLT). The center panel is electron temperature (T_e, black line), and energetic electron flux (Φ_e, gold line) measured at the same time and location as the bottom panel. The HLTs were highlighted as light orange blocks here, where the abrupt enhancements of molecular ions densities were observed. The Kp (orange bars) and Dst (red line) indices during this time of orbit 14 182 are shown for reference **(top panel)**; greyed out area on top panel corresponds to the time interval when the measurements present in bottom panel are extracted. Figure digitized and adapted from (Brinton et al., 1978).

ions through the reactions of O^+ ions with the neutral atmosphere, $O^+ + N_2 \rightarrow N + NO^+$ and possibly $O^+ + O_2 \rightarrow O_2^+ + O$. Note that the OGO 6 also had ability to distinguish the increasing ion densities of N_2^+ and O_2^+, but were not shown here due to clarity of the figure (Taylor et al., 1975). Grebowsky et al. (1983) further examined the average invariant latitude-magnetic local time (MLT) distribution of HLTs based on the OGO 6 data from 1969–1970 and found that the location of HLTs was aligned with the polar cap boundary, associated with the maximum electric convection field, as well as enhancements of soft electron fluxes.

The presence of molecular ions in the terrestrial ionosphere was also confirmed by measurements from the Ion Mass Spectrometer (IMS) on board NASA International Satellite for ionospheric Studies (ISIS 2) (Hoffman, 1970). Deployed on April 1, 1971, ISIS 2 operated in an orbit with an apogee of 1,440 km, a perigee of 1,360 km, and an inclination of 88.1°. The IMS onboard the ISIS 2 was designed to measure the ionic compositions of the ionosphere in the mass range of 1–64 amu. **Figure 5** shows such observations during the August 4, 1972 geomagnetic storm (Max Kp = 9, Min Dst = -125 nT) (Hoffman et al., 1974). These measurements indicated that during times of increased geomagnetic activity (Kp = 9), O^+ and N^+ have comparable concentrations from 55° latitude to 85° at 1,400 km altitude, while the concentration of NO^+ and N_2^+ reached more than 10^3 cm^{-3} and that of O_2^+ was ~ 10^3 cm^{-2} from 55° latitude to 70°. The ion densities ratio of NO^+/N^+ was ~ 0.015–0.35 during this event. When the spacecraft passed through above 55° latitude region, the molecular ions densities increase from 2×10^2 to 10^3 cm^{-3} and the densities of O^+ decreased from 3×10^4 to 10^4 cm^{-3}. There are several reasons that could explain the abundance of molecular ions during this time. First, based on the OGO 6 measurements from the neutral mass spectrometer in a similar event, the

densities of N_2 at high altitudes increased significantly, and this could provide a potential source of molecular N_2^+ ions (Hedin and Reber, 1972). Second, these unexpected enhancements of molecular ion densities had similar locations as those of HLTs observed by OGO 6 satellite (Taylor et al., 1975; Grebowsky et al., 1976; Grebowsky et al., 1983) and thus, the enhancement of soft electron precipitation and rapid loss of O^+ ions at a time associated with strong electric convection fields could provide an additional source of molecular ions in the topside ionosphere.

The concomitant observations of enhancements in molecular ion densities and HLTs were noted not only during solar maximum by OGO 6, but also during the solar minimum by instruments onboard the Atmosphere Explorer (AE-C) mission. Launched in December 1973, AE-C aimed to study the structure of thermosphere, especially how the photochemical processes govern the region (Richards and Voglozin, 2011). During the first year of operation, the perigee moved from about 68° latitude north down to about 60° south, and the orbit became circular at approximately 390 km altitude (Richards and Voglozin, 2011). The ion mass spectrometers on board the AE-C were a Bennett-type radio frequency ion mass spectrometer (Brinton et al., 1973) and a magnetic ion mass spectrometer (Hoffman et al., 1973), and were employed to measure ion densities.

HLTs were observed during June 1976 at 70° latitude and 300 km altitude in the southern hemisphere during quiet winter time conditions (Brinton et al., 1978). **Figure 6** shows the ion densities (bottom panel), electron temperature and energy fluxes (center panel), and the Dst and Kp indices (top; shown for context). It can be seen that at this time the density of NO^+ reached 2.5×10^3 cm^{-3}, and the density N_2^+ and O_2^+ were 9.5×10^2 and 5×10^2 cm^{-3}. Unlike the depletion of O^+ in the HLT observed by OGO 6, the observed O^+ density by AE-C didn't decrease as the molecular ion densities increased. By examining the electron temperature as well as the energetic particle flux near the HLTs, the increase of electron temperature suggests that the existence of a locally acting heating mechanism responsible for the enhancement in the energetic particle flux. This could possibly have provided the additional energy to molecular ions, leading the formation of HLTs in the high latitude ionosphere (Brinton et al., 1978). Furthermore, O^+ ions were the dominant heavy ion species above 50° latitude ionosphere and the dominant molecular ions species were either NO^+ or O_2^+. The NO^+ ions was likely to dominate the molecular ions species of the sunlit F region as well as 60°–90° latitude in the nightside region, while O_2^+ was likely to dominate the nightside region from 50°–60° latitude. Note that N_2^+ was never the dominant ion species during solar minimum conditions, but it could be the second most abundant molecular ions species where NO^+ was the major molecular ion. The highest observed density of O_2^+ and NO^+ were ~10^4 cm^{-3} near the cusp region, and ~10^3 cm^{-3} around the nightside auroral zone (Brinton et al., 1978).

The upflowing molecular ions at several thousand kilometers altitude were first observed by Suprathermal Ion Mass Spectrometer (SMS) carried on the Akebono (EXOS-D) spacecraft. Launched on February 21, 1989, the Akebono (EXOS-D) spacecraft was a Japan-led satellite mission designed to investigate processes leading to particle acceleration above the auroral region (Tsuruda and Oya, 1991). The Akebono spacecraft operated in an elliptical polar orbit, with an apogee of 2.65 R_E (~ 10,500 km) altitude, a perigee of 275 km, and inclination of 75°. The SMS on board the Akebono spacecraft was designed to measure mass-per-charge (m/q) and energy-per-charge (E/q) with the range of 1–67 amu/q and 0.1–4,000 eV/q by sampling the two dimensional thermal (0–25.5 eV) and suprathermal (55 eV/q–4.1 keV/q) ion energy distributions in the satellite spin plane (Whalen et al., 1990).

Table 1 summarizes the observations of molecular ions from Akebono spacecraft based on four storm events in 1990 [adapted from Yau et al. (1993)]. Molecular ions were a minor component of the upflowing ionospheric ion population, for which NO^+ and N_2^+ were the dominant molecular ion species, and the density of O_2^+ was one order of magnitude lower. Molecular ions could be observed during the storm main and recovery phases at altitudes between 7,000–10,000 km near 70° latitude. The abundance of molecular ions was correlated with the density ratio of N^+/O^+ (Yau et al., 1993), that is, the maximum flux of molecular ions was accompanied by the unity ratio of N^+/O^+, and the molecular ions flux could be at most 15% of the total ionospheric outflow fluxes during storm time. The increase in molecular ions densities can be explained by the increase in neutrals densities and their collisional ionization in the 500–1,000 km altitude range. For instance, the density of N_2 in this region, as predicted by the Mass-Spectrometer-Incoherent-Scatter (MSIS-86) model (Hedin, 1987), increases by a factor of ~ 80 from quiet time (Ap Index = 4) to storm time conditions (Ap Index = 60). Moreover, heavy ions produced in the 500–1,000 km altitude region are required to attain ~ 1 km/s velocities in order to reach the high altitude region. Based on the Akebono spacecraft observational data, the lifetimes of molecular ions between 300 and 1,000 km were estimated ~ tens of minutes. This implies that transverse heating commonly occurring between 400 and 1,000 km altitude during the active auroral conditions could be sufficient to energize them.

Previous observations indicated that molecular ions were likely to be present in the topside ionosphere, during and after strong geomagnetic storms, for which the minimum Dst was smaller than -100 nT. However, recent observations from the CASSIOPE Enhanced Polar Outflow Probe (e-POP) mission indicated that molecular ions were observed frequently even during modest geomagnetic storm at all e-POP altitudes, spanning between 325–1,500 km (Yau et al., 2006; Yau and Howarth, 2016). Based on the e-POP data collected during 2013–2018 time period, most observations of molecular ions occurred in the pre-midnight sector above 50° latitude ionosphere, while the lowest count rate events were located in the 8–10 MLT range, which coincided with the peak region of energetic precipitating electrons (Foss and Yau, 2019).

3 OBSERVATIONS OF MOLECULAR IONS IN THE MAGNETOSPHERE

Until the flight of the Dynamic Explorer (DE-1), instruments on board magnetospheric missions were not capable of fully resolving all heavy ion species, molecular ions in particular.

TABLE 1 | Observations of molecular ions from Akebono during four storm events in 1990, including the time and location of the observation as well as the ion fluxes of N^+ to O^+, molecular ions to O^+, and between molecular ions (NO^+:N_2^+:O_2^+). Data collected and summarized based on the Yau et al. (1993) study.

Storm event	Jan 21–23, 1990	Mar 11–13, 1990	Mar 17–19, 1990	May 25–27, 1990
Storm phase	Recovery phase	Main phase	Main phase	Recovery phase
Observed Latitude	near 70° Nightside	65°–76° Dayside	near 70° Dayside	near 70° Dayside
Observed Altitude (km)	8,700–9,950	6,100–8,160	9000–10,000	6,500–7,800
Flux of N^+/O^+	~ 0.08	~ 1	~ 0.6	~ 1
(Molecular ions)/O^+	~ 0.05	0.14	~ 0.05	0.1
Flux of NO^+:N_2^+:O_2^+	0.3: 1: 0.01	1: 0.9: 0.05	1: 0.9: 0.08	1: 1: 0.1
Min. Dst (nT) during Storm phase/Storm Event	–32/–45	–159/–162	–43/-67	–68/–87
Kp/Max Kp	4/4	7/7	6/6	6/7

TABLE 2 | AMPTE observations of molecular ions during three storm events in 1984, including the observed time intervals and spatial locations, ions energy densities, and the total molecular ions to O^+ flux ratios, with the corresponding Dst and Kp. Data collected and summarized based on the Klecker et al. (1986) study.

	Sep 4, 1984	Oct 19, 1984	Nov 17, 1984
Observed time	Onset phase	Recovery phase	Late recovery phase
Total energy density (keV/cm^3)	32	6	5.1
O^+ energy density (of total)	21%	12%	8.5%
(NO^++O_2^+)/O^+ flux (160 keV)	0.031 ± 0.004	0.018 ± 0.004	< 0.038
L	6.6–8.3	8.0–9.4	7.7–9.5
Dst/Minimum Dst (nT)	–58/–162	–60/–86	–60/–133
Kp/Max Kp	8/8	5/7	4/8

Explorer 45, launched on November 15, 1971, reported on the presence of an unexpected heavier ion species (M/Q ≥ 9) with energies in the range of tens of MeVs, observed in the radiation belt region during the geomagnetic storm of August 4, 1972 (Max Kp = 9, Min Dst = -125 nT). Because the heavy ion detector telescope on the Explorer 45 didn't have capability to accurately determine the mass of the observed ion species, Spjeldvik and Fritz (1981) identified these energetic ion species either as the magnesium, or silicon and iron ions.

Molecular N_2^+, NO^+, and O_2^+ ions were first observed in the magnetosphere by the Retarded Ion Mass Spectrometer (RIMS) (Chappell et al., 1982) on board the Dynamic Explorer (DE-1) (Craven et al., 1985). Launched on August 3, 1981, the DE-1 covered the altitude range between 500 km and ~ 3.6 Earth radii, and aimed to investigate in the interactive processes in the Earth's ionosphere, plasmasphere, and magnetosphere. RIMS was designed to measure ions with mass between 1 and 32 amu, and with energies ranging from 0 to 50 eV. To resolve molecular ions species and their corresponding kinetic energies, RIMS was designed with the mass voltage steps closer together for mass range between 28 and 32. During the storm of September 6, 1982 (Max Kp = 9, Min Dst = ~ -300 nT), DE-1 measurements show that the maximum flux of molecular ions was as high as ~ 10^6 cm^{-2} s^{-1} around 70° latitude at 1–3 R_E, and NO^+ and N_2^+ were the dominant molecular ions species with similar fluxes. Furthermore, the velocity distribution of molecular ions followed a Maxwellian distribution in the ionosphere, and transferred to the field-aligned velocity distribution at several Earth radii altitude (Craven et al., 1985). In the region between 1–3 R_E, the velocities of molecular ions were observed to be around 5–10 km/s, and their kinetic energies were at least 20 eV at 2.5 R_E geocentric distance. The DE-1 observational dataset suggests that molecular ions are likely to be produced in the polar cusp region and convected to the nightside cusp and polar cap region by the influence of crossed electric and magnetic fields (**E** × **B**).

Energetic molecular ions with energies higher than 100 keV/e were first detected in the outer ring current region (L ~ 7) by Suprathermal Energy ionic Charge Analyzer (SULEICA) onboard the Active Magnetospheric Particle Tracer Explorers (AMPTE) Ion release Module (IRM) spacecraft. Launched on August 16, 1984, the AMPTE/IRM operated in an elliptical orbit with inclination of 28.8° with an apogee of 18.7 R_E (Mobius et al., 1985). The SULEICA instrument was a curved plate electrostatic energy-per-charge analyzer that measured ion energies between 5–270 keV/q (Hausler et al., 1985). While no observations of molecular ion were reported during quiet time periods by the AMPTE/IRM spacecraft, molecular ions in the outer ring current were observed during multiple storm events (Klecker et al., 1986). **Table 2** presents a synthesis of measured (NO^++O_2^+)/O^+ fluxes, and the relevant information regarding each storm interval (Dst, Kp, and observation time interval), as well as the ratio of O^+ energy flux to the total observed energy flux for these events. The observational record indicates that both O_2^+ and NO^+ were the dominant molecular ions species in this region. The average molecular ions flux was observed to be around 3–4% of O^+ flux in the energy range 80–230 keV during active times. **Figure 7** shows the change in energy flux with particle energy during the

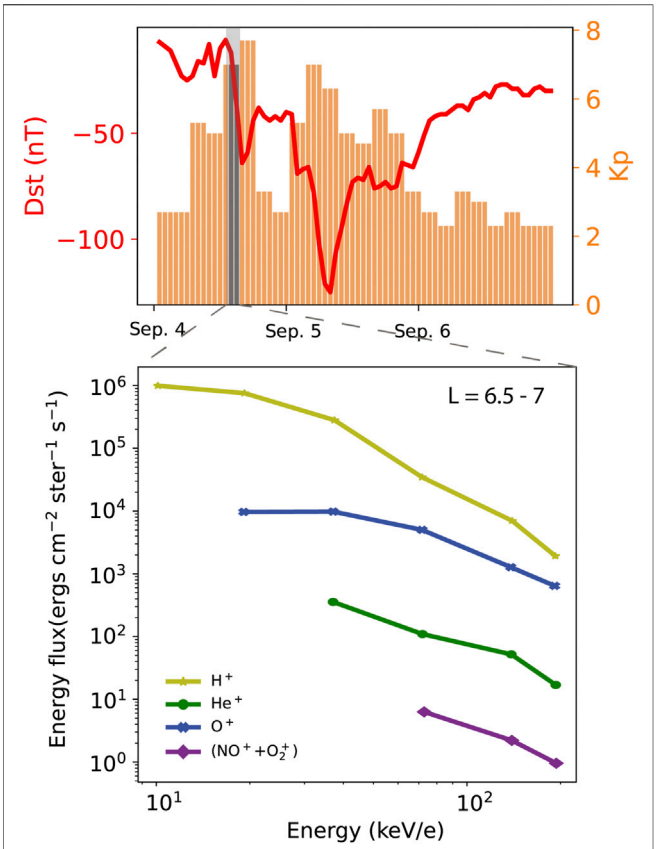

FIGURE 7 | Measurements from the SULEICA instrument on board the AMPTE/IRM spacecraft showing the energy spectra of H^+ (light green), He^+ (dark green), O^+ (blue), and molecular ions (purple) with energy range 10–230 keV/e **(bottom panel)**. The Kp (orange bars) and Dst (red line) indices from the September 4, 1984 storm are shown for reference **(top panel);** greyed out area on top panel corresponds to the time interval when the measurements presented in bottom panel are extracted. Figure digitized and adapted from (Klecker et al., 1986).

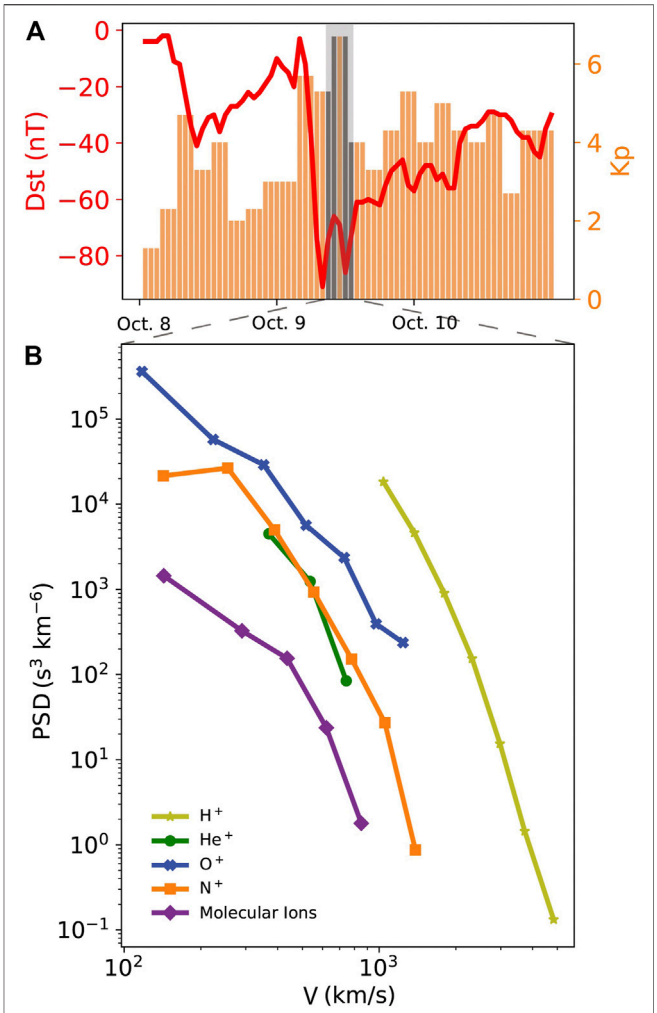

FIGURE 8 | Phase space densities (PSD) of N^+ (orange line), O^+ (blue line), and molecular ions (purple line) in the rest frame speed (v) for the interval 0958–018 and 1252–1330 UT during the storm of October 9, 1993, measured by the Geotail spacecraft **(B)**. The Kp (orange bars) and Dst (red line) indices during this storm are shown for reference **(A)**; greyed out area on top panel corresponds to the time interval when the measurements in bottom panel are extracted. Figure digitized and adapted from (Christon et al., 1994).

early main phase of the September 4, 1984 storm, based on SULEICA measurements (Klecker et al., 1986). Molecular NO^+ and O_2^+ ions (purple) were observed at L ~ 6.5–7, having energies of the order of 100 keV/e, contributing ~ 0.5% of the total energy of 32 keV/cm^{-3} in the energy range 20–230 keV/e. These observations of energetic molecular ions suggest that either the mass selection energization mechanisms or the density profile of the thermosphere during the storm time played a significant role in the efficient heating of the molecular ions as they were transported from the ionosphere to the magnetosphere.

Observations of molecular ions at hundreds of Earth radii downtail were first recorded by instruments onboard the Geotail mission (Nishida, 1994). The Suprathermal Ion Composition Spectrometer (STICS) of Geotail/EPIC (Energetic Particles and Ion Composition) instrument and the Low Energy Particle Energy Analyzer (LEP-EA) had the capability to measure ions in the energy range of 9.4–210 keV/e and 0.03–40 keV/e (Christon et al., 1994; Williams et al., 1994). Total kinetic energy, energy-per-charge, and time-of-flight measurements of individual ions are combined with various telescope parameters to generate pulse height analysis (PHAs) events and the count rates of PHAs were related to the abundances of ions in the observed region. Singly charged heavy ions, including atomic N^+ and O^+, and molecular N_2^+, NO^+, and O_2^+ ions, were observed in Earth's magnetotail at distances X ~ -146 R_E during geomagnetically active times (maximum Kp value was ~7, minimum Dst was only -40 nT). **Figure 8** shows the rest frame phase space ion densities vs. ion velocities based on Geotail observational data. It can be seen that the atomic N^+ and O^+ as well as molecular ions had relatively high velocities ~ 200–900 km/s in the rest frame of the tailward bulk plasma flow, where N^+/O^+ = ~ 25–30% and $(N_2^+ + NO^+ + O_2^+)/O^+$ = ~ 1–2%. In addition, the molecular ions observed at magnetosphere had similar velocity distribution as the atomic N^+ and O^+ in the

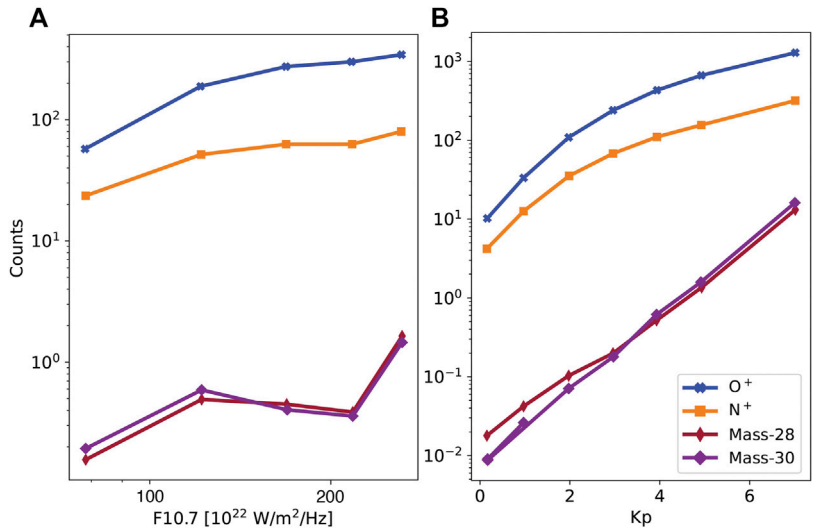

FIGURE 9 | Geotail measurements of suprathermal (~87–212 keV/e) N^+ (orange line), O^+ (blue line), and molecular ions (magenta and purple lines). Data shows average phase count rates over 3 h vs. Kp **(A)** and vs. F10.7 **(B)** indices covering observations made between 1995 and 2015. Figure digitized and adapted from (Christon et al., 2020).

outer magnetosphere (X ~ -146 R_E), but their densities were around two orders of magnitude lower.

Statistical studies based on 20 years of Geotail/STICS data (1995-2015) indicated that the relative abundance of molecular ions in the Earth's magnetosphere is ~43% N_2^+, ~47% NO^+ and ~ 10% O_2^+ (Christon et al., 2020). **Figure 9**, adapted from Christon et al. (2020), shows the variation in N^+ (orange line), O^+ (blue line) and molecular ions with mass 28 amu (magenta line) and mass 30 amu (purple line) count rates with F10.7 (left panel) and Kp (right panel) indices. These data show that the count rates of magnetospheric molecular ions are the most sensitive to geomagnetic activity, and increase faster with larger values of Kp. Moreover, the count rates of molecular ions and atomic N^+ and O^+ ions seem to indicate a different response to the F10.7 index; while the count rates of atomic N^+ and O^+ ions proportionally increased with F10.7, that of the molecular ions showed a decline for F10.7 ~ $120 \times 10^{22} - 220 \times 10^{22}$ W/m^2/Hz, and increased significantly at the highest F10.7.

Molecular ions have also been observed by the Toroidal Imaging Mass-Angle Spectrograph (TIMAS) on board the Polar satellite. Launched on February 24, 1996, the Polar spacecraft measured plasma properties in the polar ionosphere and magnetosphere, aiming to develop an understanding of the deposition of particle energy in the ionosphere and upper atmosphere (Shelley et al., 1995). The Polar spacecraft entered the orbit with an apogee of 9.0 R_E, a perigee of 1.8 R_E, and the inclination of 86°. The Polar/TIMAS instrument aimed to measure particles with energy between 15 eV/e–33 keV/e (Shelley et al., 1995). The mass spectra from TIMAS have been analysed with the help of color-coded count rates versus time and mass step at all energy channels, which allowed the separation of molecular ions from atomic O^+ and N^+ ions. However, due to the detection limit of the instrument, for particles with energies below 5 keV/e, the N_2^+, NO^+, and O_2^+ ions were not successfully distinguished (Lennartsson et al., 2000). A statistical study based on the first 22 months of data from TIMAS showed that the energy distribution of molecular ions were identical with O^+ ions, with the typical energy between 15–110 eV. However, the differential fluxes of molecular ions, ~ 10^5 cm^{-2}s^{-1}, were two orders of magnitude lower than that of O^+ ions. Furthermore, the detection frequency of molecular ions was determined to be more sensitive with the enhanced geomagnetic activity, than the O^+ detection. Therefore, the pathway and energization mechanisms of molecular ions were different from those of O^+, as they seem to be more specifically associated with enhanced geomagnetic activity (Lennartsson et al., 2000).

Surprisingly, molecular ions had been observed by the Acceleration, Reconnection, Turbulence, and Electrodynamics of the Moon's Interaction with the Sun (ARTEMIS) spacecraft, whose orbit is centered around the Moon, with periselene between 10–1,000 km and aposelene of 20,000 km (10 lunar radii) (Angelopoulos, 2010). Based on measurements from the electrostatic analyzer (ESA), Poppe et al. (2016) analyzed the ion composition data around 60 R_E away from the Earth during the storm of October 1, 2012 (Max Kp = 7, Min Dst = −122 nT) and storm of February 16, 2014 (Max Kp = 6, Min Dst = −119 nT). This study revealed that the fluxes of molecular ions were on the order of 10^5–10^6 cm^{-2} s^{-1}, while the proton fluxes were found to yield ~ 10^6–10^8 cm^{-2} s^{-1}, suggesting that molecular ions might have comparable velocities with those of protons. These observations of energetic molecular ions from ARTEMIS hint to the connection between Earth's ionospheric outflow and the composition of lunar exosphere, since the Earth could possibly deliver the nitrogen and oxygen components to the lunar volatile inventory (Poppe et al., 2016).

Recent observations based on the data from the Arase (Exploration of energization and Radiation in Geospace, ERG) satellite reveal frequent presence of molecular ions in the inner

magnetosphere during storm times. Launched on December 20, 2016, the Arase (ERG) satellite was designed to directly observe high energy particles in the magnetosphere (Miyoshi et al., 2018). The low-energy particle experiments-ion mass analyzer (LEPi) (Asamura et al., 2018) and medium-energy particle experiments-ion mass analyzer (MEPi) (Yokota et al., 2017) on board the Arase (ERG) satellite were capable of measuring the three-dimensional velocity distribution of ions in the energy range of 0.01–25 keV/q as well as 10–180 keV/q with ions species discrimination, including N^{++}/O^{++}, N^{+}/O^{+}, and $N_2^+/NO^+/O_2^+$. Based on the molecular ions measurements by LEPi and MEPi from March to December 2017, including 11 geomagnetic storms, molecular ions were frequently observed at L = 2.5–6.6 with energies above ~ 12 keV during most magnetic storms, and the average energy density ratio of the molecular ions to O^+ was found to be ~ 3% (Seki et al., 2019). The high occurrence rate of molecular ions in the inner magnetosphere indicates that fast ion outflows occur more frequently than expected during the storm time, while previous studies assumed the molecular ions were only observed during intense storms (the minimum Dst ≤ -100 nT).

The convection and energization mechanisms of molecular ions are likely to be different between the high-altitude ionosphere and magnetosphere. The molecular ions were observed to follow the similar energy distribution to O^+ by the Polar/TIMAS instrument (Lennartsson et al., 2000), but had similar velocity distribution to O^+ as observed by the Geotail/EPIC instrument and the ARTEMIS spacecraft (Christon et al., 1994; Poppe et al., 2016). In the high-altitude ionosphere, both O^+ and molecular ions with the escape energy (≥10 eV) can overcome the gravitational bound and flow out the Earth's ionosphere. Therefore, the energy distribution of these outflowing O^+ and molecular ions will be likely similar. On the other hand, O^+ and molecular ions in the magnetotail are possibly energized by the earthward $\mathbf{E} \times \mathbf{B}$ transport, which are charge and mass independent. Thus, O^+ and molecular ions can likely follow a similar velocity distribution in the magnetotail region.

Instrument limitations on board these spacecrafts brought some difficulties to the study of the cold plasma and the behavior of minor ion species in the ionosphere-magnetosphere system. For example, the minimum detection densities of ions for OGO and AE spacecrafts were 10 cm^{-3} and thus, the region with the molecular ions densities ≤10 cm^{-3} couldn't be detected. In addition, measurements of cold molecular ions in the magnetosphere are particularly difficult due to spacecraft surface charging, as the ions energy ≤10 eV had the difficulty to be fully resolved by the instruments. Nevertheless, multiple studies report on their occurrence both in the ionosphere and the magnetosphere, spanning a large energy range and radial distances.

4 DISCUSSION

Although several observations reveal that molecular ions are frequently observed in the high-latitude ionosphere and the magnetosphere, having energies of the order of eV to keV, the source and energization mechanisms leading to the outflow of these molecular ions in response to various geomagnetic conditions, are not yet fully understood. In this section, we will further explore the source and energization of outflowing molecular ions in the Earth's ionosphere-magnetosphere system.

4.1 Source of Molecular Ions

Molecular ions outflowing from the polar wind are mainly produced in the ionosphere F2 layer through the Suprathermal Electron (SE) production, including photoionization and secondary electron impact, and ion-neutral-electron chemical reactions. In this section, we provide the altitude profile of production and loss processes for all relevant polar wind molecular ions from 200–1,000 km altitude. The profiles are obtained using the Seven Ion Polar Wind Outflow Model (7iPWOM) (Lin et al., 2020) with the chemical reactions rates provided by Richards and Voglozin (2011).

The 7iPWOM expanded the chemical reactions of ionospheric N^+ ions in the ionosphere F2 layer, and SE production for all seven ion species, including O^+, N^+ and three molecular ion species, based on the GLobal airglOW (GLOW) model (Solomon et al., 1988; Glocer et al., 2012) and the cross-sectional area of the neutral-electron collision provided by (Gronoff et al., 2012b,a). The neutrals number density are obtained from NRLMSISE-00 empirical model. However, the 7iPWOM included neutral NO, $NO(^2D)$, $N(^2D)$ and $N(^4S)$ density based on the neutral density of the simulation results from the Global ionosphere Thermosphere Model (GITM) (Ridley et al., 2006).

The chemistry scheme of the 7iPWOM includes all relevant reactions with the chemical reactions rates provided by Richards and Voglozin (2011). Since the charge exchange between $O^+(^2D)$ and N_2 is the main source to produce N_2^+ in the ionosphere above 200 km altitude (Torr and Orsini, 1978), the 7iPWOM calculates this charge exchange reaction rate by deriving $O^+(^2D)$ from the Global ionosphere Thermosphere Model (GITM). In order to illustrate the influence of solar conditions to the molecular ions chemistry, we present here the production and loss rate of the molecular ions based on the steady state of the 7iPWOM quiet time solution during the Solar Maximum ($F10.7 = 180 \times 10^{-22}$ WHz/m^2) and Minimum ($F10.7 = 80 \times 10^{-22}$ WHz/m^2) summer noon, shown in **Figure 10**. The steady state of summer noon conditions are represented by the solution of a single field line, for which the foot point is located in 80° latitude and 12 MLT, initialized for 24 h to achieve steady state. Since molecular ions became the minor ion species above 1,000 km, and their detection in the polar wind during the quiet times at this altitude was reported to be challenging (Craven et al., 1985; Christon et al., 1994), here we only present the altitude profiles for molecular ions production and loss at 200–1,000 km altitudes.

The right-hand side of **Figure 10** shows the various chemical reactions contributing to the production and loss of N_2^+ (top row), NO^+ (center row), and O_2^+ (bottom row). Each column represents the simulation results of 7iPWOM during Solar Maximum and Solar Minimum from left to right. The production of molecular N_2^+ (dark red line), NO^+ (purple line), O_2^+ (brown line) ions takes place via photoionization, secondary electron impact, and various ion-neutral-electron chemical reactions, while the losses of molecular ions (grey lines) occur either via dissociative

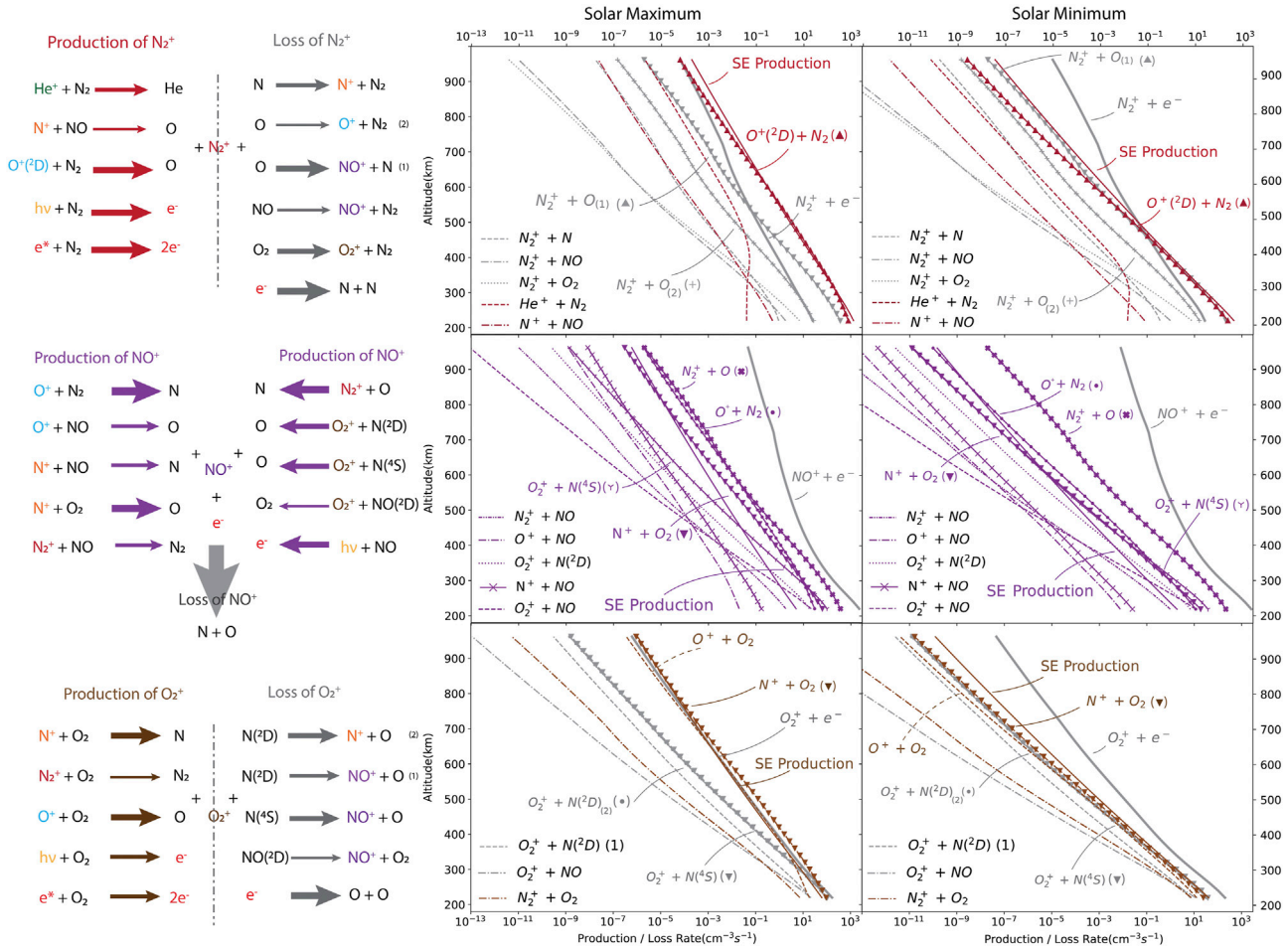

FIGURE 10 | Comparison of ion production (colored lines) and loss (grey lines) reactions between 200 and 1,000 km altitude range, based on the 7iPWOM simulation results during solar maximum **(left column)** and minimum **(right column)** summer noon. The diagram on the left-hand side shows various chemical reactions of productions and losses of molecular ions and the thickness of the arrows represents the magnitude of reactions rates ($cm^{-3}s^{-1}$).

recombination with e^- to form the neutral species or via various ion-neutral-electron chemical reactions. The diagrams on the left-hand side of **Figure 10** list the relevant ionospheric chemistry related to molecular N_2^+ (dark red), NO^+ (purple), O_2^+ (brown) ions. The participating ion species are marked by colored text, including O^+ (blue), N^+ (orange), He^+ (dark green) and e^- (red). The colored arrows represents the chemical production of molecular ions, while the grey arrows show their losses via chemical reactions. The thickness of these arrows indicates the efficiency of said reaction rates based on the quiet time simulation results of the 7iPWOM (right-hand side of **Figure 10**). Below, we will further explore the ionospheric chemistry of each molecular ion species.

4.1.1 The Ionospheric Chemistry of N_2^+

During Solar Maximum conditions, the main contributors to the production of N_2^+ ions in the altitude range of 200–1,000 km are the SE production (dark red solid line) and the charge exchange between $O^+(^2D)$ and N_2 (dark red triangle line). N_2^+ are mostly lost due to dissociative recombination with electrons and charge exchange between N_2^+ and neutral O species, reactions that are leading to the production of N, and N_2 neutral species, and NO^+ and O_2^+ ions. During Solar Maximum condition, the production and loss rates of N_2^+ varied more than from Solar Minimum case. Therefore, during Solar Minimum, the N_2^+ production rates via SE production and the charge exchange between $O^+(^2D)$ and N_2 could impede the losses of N_2^+ from dissociative recombination (grey dashed line) during the Solar Maximum, while these two production rates of N_2^+ were only larger than dissociative losses of N_2^+ below 500 km during Solar Minimum.

4.1.2 The Ionospheric Chemistry of NO^+

NO^+ is produced through a multitude of chemical reactions, with rates largely affected by the solar activity. The production rates of NO^+ due to charge exchange between N_2^+ and O (purple cross marker line) and charge exchange between O^+ and N_2 (purple dotted line) were comparable during Solar Maximum; however, the reaction rate of charge exchange between N_2^+ and O was at least one order of magnitude than other reactions during Solar Minimum. The SE production of NO^+ is not very important both

during the solar maximum and minimum as it is only the third or fourth important reactions, which followed the same conclusion of NO^+ ionospheric chemistry by the study of Richards and Voglozin (2011). Moreover, dissociative recombination rates of NO^+ (grey solid lines) was the only reaction to remove NO^+ from the ionosphere F2 layer. Since the dissociative recombination rate of NO^+ was generally one order of magnitude larger at the low altitude and five orders of magnitude larger at 1,000 km altitude, the NO^+ ions densities decreased substantially from 200 to 1,000 km altitude.

4.1.3 The Ionospheric Chemistry of O_2^+

The loss of O_2^+ ions in the ionosphere F2 layer is due to the dissociative recombination with electrons (grey solid line), and the loss of O_2^+ produces the neutral O species and molecular NO^+ ions, with minor N^+ ions species. Similar to the case of N_2^+ ions, solar activity also alters the ionospheric chemistry of O_2^+ ions. During Solar Maximum condition, the O_2^+ production rates due to the SE production (brown solid line) and the charge exchange of O^+ or N^+ ions with the neutral O_2 (brown dashed and triangle lines), could impede the O_2^+ losses of dissociative recombination. However, during Solar Minimum, the dissociative recombination can be at least one order of magnitude larger than the production rates of O_2^+.

The above analysis of the productions and losses of molecular NO^+, N_2^+ and O_2^+ ions between 200–1,000 km altitude range with the observations results in **Sections 2**, **3**, we can conclude that:

- The SE productions of molecular N_2^+, NO^+, O_2^+ are not the dominant chemical reactions for the production of NO^+ and O_2^+ in the ionosphere F2 layer, consistent with previous findings (Richards and Voglozin, 2011).
- The chemical reactions leading to the loss of O^+ are also leading to the production of NO^+ and therefore, the presence of NO^+ leads to the increasing ratio of N^+/O^+ in the ionosphere, as observed by Hoffman et al. (1974); Yau et al. (1993); Wilson and Craven (1999).
- The chemical reactions leading to the loss of N_2^+ are also leading to the production of NO^+ and neutral N_2 species, causing an increase in the neutral N_2 density in the low-altitude ionosphere, as reported in DE-2 measurements (Wilson and Craven, 1999).

4.2 Possible Energization Mechanisms

Molecular ions are required to be energized in a very short time once produced either by the SE production or reactions with neutral species, in order to impede with their fast dissociative recombination with electrons in the ionosphere F2 layer. Ionospheric observations of molecular ions by OGO and AE spacecraft missions showed that the abrupt enhancements of molecular ions densities in the region of HLTs were often accompanied by the decrease of O^+ ion densities, and an increase in the electron temperature and energetic particle flux. Therefore, fast molecular ions outflow were produced by the rapid losses of O^+ due to strong electric field and energized by the enhancement of soft electron precipitation associated with the polar cap region in the ionosphere (Taylor et al., 1975; Grebowsky et al., 1976; Brinton et al., 1978; Grebowsky et al., 1983).

Several studies have focused on the effect of ion frictional heating (ion-neutral collisions) due to strong electric convection field (Schunk et al., 1975; Wilson and Craven, 1999; Schunk and Nagy, 2009; Zettergren et al., 2010; Zettergren et al., 2011). As ions are convected through the slower moving neutral gas with $\mathbf{E} \times \mathbf{B}$ drift, they are heated through the ion-neutral collision, which leads to an increase in the ion temperatures. This in turn facilitates an increase in the chemical reactions rates in the ionosphere, and therefore also facilitates the production of molecular ions. As the convection electric field ($E_\perp$) approaches $50\,mV\,m^{-1}$, the ion temperature substantially increases, leading to the enhancement of $O^+ + N_2 \rightarrow N + NO^+$ reaction rate. Numerical simulations suggest that when $E_\perp$ approaches to $200\,mV\,m^{-1}$, the loss of O^+ causes rapid enhancement of NO^+ ion density. Therefore, NO^+ ions could become the dominant ion species in the high-latitude ionosphere up to 600 km altitude (Schunk et al., 1975).

The ion frictional heating of molecular ions outflow due to strong convection electric field was also investigated with the near-conjunction measurement of the DE-1 and DE-2 spacecraft missions (Wilson and Craven, 1999). By selecting the events when both spacecrafts passed through similar latitudes and longitudes, measurements of neutral species composition and temperature from the low-altitude DE-2 mission (335–746 km altitude range) were analyzed in conjunction with measurements of N^+, O^+ and molecular ions densities in the high altitude region observed by the DE-1 (1,000–4,000 km altitude range). The results showed that the increased molecular ions densities observed in the high altitude region by DE-1 were always accompanied by the enhancements of ions temperatures and strong electric fields in the low altitude region by DE-2. This points out the molecular ions outflow could be sourced and energized by the strong cusp associated plasma convection, which also modified the composition of the ionosphere and thermosphere.

Studies using the European Incoherent Scatter (EISCAT) data of ion velocity and temperature also suggest that ion frictional heating plays an important role in the molecular ions upflow. Based on the frequent observations of molecular ions in the innermagnetosphere by the Arase satellite during multiple storm times (Seki et al., 2019), Takada et al. (2021) further determined the energization supplied to ionospheric molecular ions with the ion velocity and temperature data from the EISCAT Ultra High Frequency (UHF) radar (933 MHz) at Tromsø (located at ~ 70° latitude). The measurement of temperature and velocity of ions were more than 2000 K and ~ 50–150 m/s at 250–350 km altitude, and the flux of molecular ions at 350 km altitude was two orders of magnitude higher than during nominal conditions, at which time the convection electric field increased a factor of 2. By examining the momentum equation of ions, the ion and electron pressure gradients were balanced with the gravitational force and thus, the ion frictional heating could be a possible energization mechanism of low-altitude molecular ions upflow.

Molecular ions observed at 300–1,000 km altitudes were also energized by ion resonance heating, enhancement of soft electron precipitation occurring in the cusp region, or the plasma instabilities and the role of various energization mechanisms

TABLE 3 | Mission details, including the information of orbit, launch and decay date, as well as the observed density ratio of $(NO^+ + O_2^+ + N_2^+)/O^+$ during the storm time only (if not specified). ARTEMIS is currently centered at the Moon and thus, the perigee and apogee are refereed as periselene and aposelene. Cross marker, x, in a cell indicates that the data are unavailable or not relevant.

Mission	Lifetime	Orbit				Energy range	Molecular ions/O^+	References
		Perigee	Apogee	Inclination	Period			
Sputnik 3	Launch Date: May 15, 1958 Decay Date: April 6, 1960	217 km	1864 km	65.18°	105.9 min	Bennett-type radio frequency quadrupole mass spectrometer	x	Nauk and Doklady (1961); Istomin (1966)
OGO 6	Launch Date: Jun 5, 1969 Decay Date: Oct 12, 1979	413 km	1,077 km	82°	99.7 min	Bennett-type Ion Mass spectrometer	0.01–0.1	Taylor (1971); Jackson and Vette (1975); Taylor (1974); Taylor et al. (1975); Grebowsky et al. (1976, 1983)
ISIS 2	Launch Date: Apr 1, 1971 Decay Date: Oct 1, 1979	1,360 km	1,440 km	88.1°	113.6 min	Ion Mass Spectrometer	10^{-4}–0.1	Hoffman (1970); Hoffman et al. (1974)
AE-C	Launch Date: Dec 16, 1973 Decay Date: Dec 12, 1978	149 km	4,294 km	68.1°	132.3 min	Bennett Ion Mass spectrometer or Magnetic Ion Mass spectrometer	10^{-3}–0.1	Brinton et al. (1973); Hoffman et al. (1973); Brinton et al. (1978)
DE-1	Launch Date: Aug 3, 1981 Decay Date: Feb 28, 1991	488 km	23,289 km	89.9°	409 min	Retarding Ion Mass Spectrometer (RIMS) 0–45 eV	x	Chappell et al. (1982); Craven et al. (1985); Wilson and Craven (1999)
AMPTE/IRM	Launch Date: Aug 16, 1984 Decay Date: Aug 14, 1986	6,944.89 km	119,965.93 km	28.6°	2,658 min	Suprathermal Energy ionic Charge Analyzer (SULEICA) 5–270 keV/e	≤0.03	Hausler et al. (1985); Mobius et al. (1985); Klecker et al. (1986)
Akebono	Launch Date: Feb 21, 1989 Decay Date: Apr 23, 2015	275 km	10,500 km	75°	211 min	Suprathermal Ion Mass Spectrometer (SMS) 0–25.5 eV; 55 eV/q–4.1 keV/q	≤0.1	Tsuruda and Oya (1991); Whalen et al. (1990); Yau et al. (1993); Peterson et al. (1994)
Geotail	Launch Date: July 24, 1992	51,328 km	190,664 km	10.51°	7,539.86 min	Suprathermal Ion Composition Spectrometer (STICS) 9.4–210 keV/e	Energy Flux ≤10^{-3}	Nishida (1994); Christon et al. (1994); Williams et al. (1994); Christon et al. (2020)
Polar	Launch date: Feb 24, 1996 Deactivated Date: Apr 28, 2008	185 km	50,551 km	85.9°	938.1 min	Toroidal Imaging Mass-Angle Spectrograph (TIMAS) 0–40 KeV/e	≤10^{-2}	Shelley et al. (1995); Lennartsson et al. (2000)
ARTEMIS (THEMIS B and C) (centered at Moon)	Launch date: Feb 17, 2007	~ 10–1,000 km	~ 20,000 km	x	1,650 min	Electrostatic Analyzer (ESA) 5 eV–25 keV	x	Angelopoulos (2010); Poppe et al. (2016)
e-POP	Launch Date: Sept 29, 2013	325 km	1,500 km	81°	103 min	Imaging and Rapid-Scanning Ion Mass Spectrometer (IRM); measures the composition and 3-dimensional velocity distributions of low-energy (1–90 eV/e) ions in the mass-per-charge (M/q) range of 1–40 AMU/e	x	Yau et al. (2006); Yau and Howarth (2016); Foss and Yau (2019)

(Continued on following page)

TABLE 3 | (*Continued*) Mission details, including the information of orbit, launch and decay date, as well as the observed density ratio of $(NO^+ + O_2^+ + N_2^+)/O^+$ during the storm time only (if not specified). ARTEMIS is currently centered at the Moon and thus, the perigee and apogee are refereed as periselene and aposelene. Cross marker, x, in a cell indicates that the data are unavailable or not relevant.

Mission	Lifetime	Orbit				Energy range	Molecular ions/O^+	References
		Perigee	Apogee	Inclination	Period			
Arase (ERG)	Launch Date: Dec 20, 2016	460 km	32,110 km	31°	565 min	Medium-energy particle ion mass analyzer (MEPi) 7–87 keV and low-energy particle experiments-ion mass analyzer (LEPi) 0.01–25 keV/q	Energy Density ≤0.03	Miyoshi et al. (2018); Asamura et al. (2018); Seki et al. (2019)

acting on the molecular ion populations in the 300–500 km altitude during multiple storm times were examined by Peterson et al. (1994). This study estimated that in this region, the lifetime of molecular ions due to recombination reactions is about few minutes, but the time needed to acquire sufficient escape energy (~ 10 eV) at the 400 km, solely by the ion frictional heating or resonance heating, was at least one order of magnitude more than the lifetime of molecular ions. Therefore, we currently lack a robust understanding of the possible mechanisms responsible to the acceleration of these heavy ions species.

4.2.1 Unresolved Issues of Energization Mechanisms of Fast Molecular Ions Outflow

The observed outflow of molecular ions implies the existence of energization mechanisms that can provide the additional escape energy (of at least ~10 eV) at comparable timescales with losses of molecular ions, and it is likely that these potential energization mechanisms are acting concomitantly, even though they might take place at different altitudes. However, the relative contributions of these energization mechanisms responsible for the molecular ions outflow are still difficult to assess due to the scarceness of observations, also linked to instrument limitations. For example, observations of particle precipitation with energies up to 1 keV by the Low Altitude Plasma Instrument (LAPI) on board the DE-2 were concurrent with the observation of molecular ions in the high altitude ionosphere (Wilson and Craven, 1999). Moreover, it has been suggested that the ionospheric plasma instabilities driven by magnetospheric electron precipitation could possibly energize molecular ions in the ionosphere (Peterson et al., 1994). However, due to the small scales of particle precipitation as well as low frequency waves, the instruments on board the DE-2 and Akebono couldn't resolve the spectrum with such high resolution.

There is also a need for additional observations of molecular ions in the magnetosphere, in order to understand the mechanisms responsible for their energization from eVs to keVs. Observations of molecular ions indicate that they could achieve ~ 5 eV at 4,000 km altitude, but their escape energies are typically between 10–20 eV. This indicates that outflowing molecular ions need to acquire additional 5 eV above 4,000 km altitude (Wilson and Craven, 1999). Moreover, the molecular ion energies could be observed up to 100 eV in the high-altitude ionosphere (Lennartsson et al., 2000) and 100 keV in the outer magnetosphere (Christon et al., 1994). This suggests that the further energization mechanisms of molecular ions takes place in the magnetosphere as well. Furthermore, the observed molecular ions in the high-latitude ionosphere had similar energy distributions to that of O^+ ions (Lennartsson et al., 2000). This indicates that outflowing molecular ions in the ionosphere are required to obtain more energy than outflowing O^+ ions, most likely by the mass selection mechanisms that heat the heavier ions preferentially.

One possible mass selection mechanisms to energize the molecular ions preferentially above 1,000 km is the resonant wave-particle interaction (WPI), which is considered to be a major pathway of ion heating and acceleration, both in the cusp and auroral region (Andre and Yau, 1997). The energization of ion outflow via WPI is caused by the electric field perturbation, perpendicular to the magnetic field, which leads to an increase in the ion perpendicular velocity in a very short time. Therefore, these energized particles move upward along the field lines and form ion conics, due to the acceleration by magnetic mirror force. The gyro-frequency of ions, inversely proportional to the mass, is resonant with the low frequency wave, meaning that molecular ions are preferentially heated via WPI. Although the efficacy of WPI in the energization of molecular ion species remains largely unknown, several studies addressed the energization of O^+ ions via WPI. For example, multiple observations from the Akebono, Interball-2 and Cluster satellites report on the abrupt energization of O^+ from 10 eV to 10 keV at 4.3 R_E in 10 min (Bouhram et al., 2004). Quasi-linear theory supports the hypothesis that the abrupt enhancements of O^+ energy along the magnetic field lines are due to WPI (Crew et al., 1990). Since the diffusion coefficient is inversely proportional to the mass of ions, molecular ions are expected to be preferentially energized by the resonant WPI.

5 CONCLUSION

Table 3 summarizes the existing observational data sets of molecular ions from past and currently operating spacecraft missions, covering altitudes from few hundred kilometers to hundreds of Earth radii. These observations of molecular ions in the ionosphere-magnetosphere system suggest that:

1. The densities of molecular ions in the polar ionosphere at altitudes between 200–1,000 km were reported to be 0.1–1% of O^+ densities; however, during geomagnetically active times, the abrupt enhancement of molecular ions densities in the high latitude troughs (whose latitudes were aligned with auroral activity) could reach about 10% of O^+ ion densities.
2. The possibility of detecting molecular ions in the magnetosphere was nearly zero during the quiet times; however, during geomagnetically active times they were frequently detected both in the inner and outer magnetosphere. The molecular ions fluxes were generally less than two orders of magnitude than that of O^+.
3. The increase in molecular ions densities or fluxes were often accompanied by a high ratio of N^+/O^+ in the ionosphere-magnetosphere system. This indicates that the presence of molecular ions could impact the abundances of N^+ and O^+ ions, and can act as a reference to investigate the energization of heavy ions in the polar wind.

Magnetospheric molecular ions were only observed during the storm times, and thus, the observations of molecular ions in the high altitude region are very scarce. This leads to very little knowledge on the convection and energization of molecular ions, causing lack of understanding of their behavior and dynamics both at low and high altitudes. There seems to be an increase in the molecular ions observations in the past 10 years, probably linked to improved mass resolution on instruments flying on current space missions. However, these observational data all occurred at the solar cycle 24, and couldn't fully represent the molecular ions dynamics in the Earth's magnetosphere-ionosphere system. Therefore, a dedicated geospace mission that would measure various plasma properties and provide detailed composition in the geospace, at all altitudes, is required in order to understand the relative contributions and the various energization mechanisms of these molecular ions throughout geospace.

Additionally, understanding the sources, energization mechanisms, and the overall dynamics of molecular ions in the magnetosphere-ionosphere system could possibly help understand the impact of the minor heavy ion species in the magnetosphere. Cluster (Haaland et al., 2021) and Geotail (Christon et al., 2017) missions have reported the observations of metal ions in the magnetosphere, but the sources and the transport mechanisms of these metal ions are still largely unknown. This review paper is intended to help inform and guide future ionosphere and magnetosphere studies, and provides context for the available observations of molecular ions. Knowledge of the different behaviors and paths of energization of heavy ions such as N^+, O^+, and molecular ions will play a crucial role in the interpretations and analysis of data from many current space missions.

AUTHOR CONTRIBUTIONS

All authors listed have made a substantial, direct, and intellectual contribution to the work and approved it for publication.

FUNDING

Work at University of Illinois at Urbana-Champaign was performed with financial support from AFOSR YIP award no. AF FA 9550-18-1-0195, and the NASA grants N99066ZO, 80NSSC20K1231, 80NSSC21K1425, and 3004631577. The PWOM model has been included in the Space Weather Modeling Framework, which is available for download (at http://csem.engin.umich.edu/tools/swmf/downloads.php). The simulation results of the GITM model has been available in the Community Coordinated Modeling Center (CCMC) webpage (at https://ccmc.gsfc.nasa.gov/models/modelinfo.php?model=GITM).

ACKNOWLEDGMENTS

The authors would like to thank the reviewers for their valuable comments and suggestions to improve the quality of the paper. The authors also thank HeRA team member Hsinju Chen for helpful suggestions and discussions on the paper.

REFERENCES

André, M., and Yau, A. (1997). Theories and Observations of Ion Energization and Outflow in the High Latitude Magnetosphere. *Space Sci. Rev.* 80, 27–48. doi:10.1007/978-94-009-0045-5_2

Angelopoulos, V. (2010). The Artemis mission. *Space Sci. Rev.* 165, 3–25. doi:10.1007/s11214-010-9687-2

Asamura, K., Kazama, Y., Yokota, S., Kasahara, S., and Miyoshi, Y. (2018). Low-energy Particle Experiments-Ion Mass Analyzer (LEPi) Onboard the ERG (Arase) Satellite. *Earth Planets Space* 70, 70. doi:10.1186/s40623-018-0846-0

Axford, W. I., and Hines, C. O. (1961). A Unifying Theory of High-Latitude Geophysical Phenomena and Geomagnetic Storms. *Can. J. Phys.* 39, 1433–1464. doi:10.1139/p61-172

Barakat, A. R., and Schunk, R. W. (2006). A Three-Dimensional Model of the Generalized Polar Wind. *J. Geophys. Res.* 111, A12314. doi:10.1029/2006ja011662

Bouhram, M., Klecker, B., Miyake, W., Rème, H., Sauvaud, J.-A., Malingre, M., et al. (2004). On the Altitude Dependence of Transversely Heated O+ Distributions in the Cusp/cleft. *Ann. Geophys.* 22, 1787–1798. doi:10.5194/angeo-22-1787-2004

Brinton, H. C., Grebowsky, J. M., and Brace, L. H. (1978). The High-Latitude WinterFRegion at 300 Km: Thermal Plasma Observations from AE-C. *J. Geophys. Res.* 83, 4767–4776. doi:10.1029/ja083ia10p04767

Brinton, H. C., Scott, L. R., Pharo, M. W., III, and Coulson, J. T. (1973). The bennett Ion-Mass Spectrometer on Atmosphere Explorer-C and -e. *Radio Sci.* 8, 323–332. doi:10.1029/RS008i004p00323

Chappell, C. R., Olsen, R. C., Green, J. L., Johnson, J. F. E., and Waite, J. H. (1982). The Discovery of Nitrogen Ions in the Earth's Magnetosphere. *Geophys. Res. Lett.* 9, 937–940. doi:10.1029/gl009i009p00937

Christon, S. P., Gloeckler, G., Williams, D. J., Mukai, T., McEntire, R. W., Jacquey, C., et al. (1994). Energetic Atomic and Molecular Ions of Ionospheric Origin Observed in Distant Magnetotail Flow-Reversal Events. *Geophys. Res. Lett.* 21, 3023–3026. doi:10.1029/94GL02095

Christon, S. P., Hamilton, D. C., Mitchell, D. G., Plane, J. M. C., and Nylund, S. R. (2020). Suprathermal Magnetospheric Atomic and Molecular Heavy Ions at and Near Earth, Jupiter, and Saturn: Observations and Identification. *J. Geophys. Res. Space Phys.* 125, e27271. doi:10.1029/2019ja027271

Christon, S. P., Hamilton, D. C., Plane, J. M. C., Mitchell, D. G., Grebowsky, J. M., Spjeldvik, W. N., et al. (2017). Discovery of Suprathermal Ionospheric Origin Fe+ in and Near Earth's Magnetosphere. *J. Geophys. Res. Space Phys.* 122, 175–200. doi:10.1002/2017JA024414

Craven, P. D., Olsen, R. C., Chappell, C. R., and Kakani, L. (1985). Observations of Molecular Ions in the Earth's Magnetosphere. *J. Geophys. Res.* 90, 7599–7605. doi:10.1029/JA090iA08p07599

Crew, G. B., Chang, T., Retterer, J. M., Peterson, W. K., Gurnett, D. A., and Huff, R. L. (1990). Ion Cyclotron Resonance Heated Conics: Theory and Observations. *J. Geophys. Res.* 95, 3959–3985. doi:10.1029/JA095iA04p03959

Daglis, I. A., Thorne, R. M., Baumjohann, W., and Orsini, S. (1999). The Terrestrial Ring Current: Origin, Formation, and Decay. *Rev. Geophys.* 37, 407–438. doi:10.1029/1999RG900009

Foss, V., and Yau, A. (2019). *Molecular Ions in Ion Upflows and Their Effect on Hot Atomic Oxygen Production*. Calgary, AB: University of Calgary. PhD Thesis.

Garcia, K. S., Merkin, V. G., and Hughes, W. J. (2010). Effects of Nightside O+outflow on Magnetospheric Dynamics: Results of Multifluid MHD Modeling. *J. Geophys. Res.* 115, a–n. doi:10.1029/2010JA015730

Glocer, A., Kitamura, N., Toth, G., and Gombosi, T. (2012). Modeling Solar Zenith Angle Effects on the Polar Wind. *J. Geophys. Res.* 117, a–n. doi:10.1029/2011JA017136

Glocer, A., Toth, G., and Fok, M.-C. (2018). Including Kinetic Ion Effects in the Coupled Global Ionospheric Outflow Solution. *J. Geophys. Res. Space Phys.* 123, 2851–2871. doi:10.1002/2018ja025241

Glocer, A., Tóth, G., Gombosi, T., and Welling, D. (2009). Modeling Ionospheric Outflows and Their Impact on the Magnetosphere, Initial Results. *J. Geophys. Res.* 114, a–n. doi:10.1029/2009JA014053

[Dataset] Grebowsky, J. M., Taylor, H. A., and Lindsay, J. M. (1983). *Location and Source of Ionospheric High Latitude Troughs*. Planetary and Space Science. doi:10.1016/0032–0633(83)90034-X

Grebowsky, J. M., Chen, A. J., and Taylor, H. A. (1976). High-latitude Troughs and the Polar Cap Boundary. *J. Geophys. Res.* 81, 690–694. doi:10.1029/ja081i004p00690

Gronoff, G., Simon Wedlund, C., Mertens, C. J., Barthélemy, M., Lillis, R. J., and Witasse, O. (2012a). Computing Uncertainties in Ionosphere-Airglow Models: Ii. The Martian Airglow. *J. Geophys. Res.* 117, a–n. doi:10.1029/2011JA017308

Gronoff, G., Simon Wedlund, C., Mertens, C. J., and Lillis, R. J. (2012b). Computing Uncertainties in Ionosphere-Airglow Models: I. Electron Flux and Species Production Uncertainties for mars. *J. Geophys. Res.* 117, a–n. doi:10.1029/2011JA016930

Haaland, S., Li, K., Eriksson, A., André, M., Engwall, E., FöRster, M., et al. (2012b). *Cold Ion Outflow as a Source of Plasma for the Magnetosphere*. American Geophysical Union, 341–354. doi:10.1029/2012GM001317

Haaland, S., Daly, P. W., and Vilenius, E. (2021). Heavy metal and rock in space: Cluster rapid observations of fe and si. Available at; http://resolver.sub.uni-goettingen.de/purl?gldocs-11858/8681.

Haaland, S., Eriksson, A., Engwall, E., Lybekk, B., Nilsson, H., Pedersen, A., et al. (2012a). Estimating the Capture and Loss of Cold Plasma from Ionospheric Outflow. *J. Geophys. Res. Space Phys.* 117, a–n. doi:10.1029/2012JA017679

Hausler, B., Melzner, F., Stocker, J., Valenzuela, A., Bauer, O., Parigger, P., et al. (1985). The Ampte Irm Spacecraft. *IEEE Trans. Geosci. Remote Sensing* GE-23, 192–201. doi:10.1109/TGRS.1985.289513

Hedin, A. E. (1987). MSIS-86 Thermospheric Model. *J. Geophys. Res.* 92, 4649–4662. doi:10.1029/JA092iA05p04649

Hedin, A. E., and Reber, C. A. (1972). Longitudinal Variations of Thermospheric Composition Indicating Magnetic Control of Polar Heat Input. *J. Geophys. Res.* (1896-1977) (77), 2871–2879. doi:10.1029/JA077i016p02871

Hoffman, J. H., Dodson, W. H., Lippincott, C. R., and Hammack, H. D. (1974). Initial Ion Composition Results from the Isis 2 Satellite. *J. Geophys. Res.* 79, 4246–4251. doi:10.1029/ja079i028p04246

Hoffman, J. H., Hanson, W. B., Lippincott, C. R., and Ferguson, E. E. (1973). The Magnetic Ion-Mass Spectrometer on Atmosphere Explorer. *Radio Sci.* 8, 315–322. doi:10.1029/RS008i004p00315

Hoffman, J. H. (1970). Studies of the Composition of the Ionosphere with a Magnetic Deflection Mass Spectrometer. *Int. J. Mass Spectrom. Ion Phys.* 4, 315–322. doi:10.1016/0020-7381(70)85047-1

Ilie, R., and Liemohn, M. W. (2016). The Outflow of Ionospheric Nitrogen Ions: A Possible Tracer for the Altitude-dependent Transport and Energization Processes of Ionospheric Plasma. *J. Geophys. Res. Space Phys.* 121, 9250–9255. doi:10.1002/2015ja022162

Ilie, R., Liemohn, M. W., Toth, G., Yu Ganushkina, N., and Daldorff, L. K. S. (2015). Assessing the Role of Oxygen on Ring Current Formation and Evolution through Numerical Experiments. *J. Geophys. Res. Space Phys.* 120, 4656–4668. doi:10.1002/2015JA021157.2015JA021157

Ilie, R., Skoug, R. M., Valek, P., Funsten, H. O., and Glocer, A. (2013). Global View of Inner Magnetosphere Composition during Storm Time. *J. Geophys. Res. Space Phys.* 118, 7074–7084. doi:10.1002/2012ja018468

Istomin, V. G. (1966). Observational Results on Atmospheric Ions in Region of Outer Ionosphere. *Ann. De Geophysique* 22, 255.

Jackson, J. E., and Vette, J. I. (1975). *The Orbiting Geophysical Observatories*. Washington, DC: NASA Special Publication, 7601.

Johnson, A. W., and Gerardo, J. B. (1972). Recombination and Ionization in a Molecular-Ion-Dominated Helium Afterglow. *Phys. Rev. A.* 5, 1410–1418. doi:10.1103/PhysRevA.5.1410

Klecker, B., Möbius, E., Hovestadt, D., Scholer, M., Gloeckler, G., and Ipavich, F. M. (1986). Discovery of Energetic Molecular Ions (NO+and O2+) in the Storm Time Ring Current. *Geophys. Res. Lett.* 13, 632–635. doi:10.1029/GL013i007p00632

Kronberg, E. A., Ashour-Abdalla, M., Dandouras, I., Delcourt, D. C., Grigorenko, E. E., Kistler, L. M., et al. (2014). Circulation of Heavy Ions and Their Dynamical Effects in the Magnetosphere: Recent Observations and Models. *Space Sci. Rev.* 184, 173–235. doi:10.1007/s11214-014-0104-0

Lennartsson, O. W., Collin, H. L., Peterson, W. K., and Shelley, E. G. (2000). Polar/timas Statistical Results on the Outflow of Molecular Ions from Earth at Solar Minimum. *Adv. Space Res.* 25, 2417–2420. doi:10.1016/S0273-1177(99)00531-1

Lin, M.-Y., Ilie, R., and Glocer, A. (2020). The Contribution of N+ Ions to Earth's Polar Wind. *Geophys. Res. Lett.* 47, 18. doi:10.1029/2020GL089321

Maggiolo, R., Sauvaud, J. A., Fontaine, D., Teste, A., Grigorenko, E., Balogh, A., et al. (2006). A Multi-Satellite Study of Accelerated Ionospheric Ion Beams above the Polar Cap. *Ann. Geophys.* 24, 1665–1684. doi:10.5194/angeo-24-1665-2006

Miyoshi, Y., Shinohara, I., Takashima, T., Asamura, K., Higashio, N., Mitani, T., et al. (2018). Geospace Exploration Project ERG. *Earth Planets Space* 70, 101. doi:10.1186/s40623-018-0862-0

Mobius, E., Gloeckler, G., Hovestadt, D., Ipavich, F. M., Klecker, B., Scholer, M., et al. (1985). The Time-Of-Flight Spectrometer Suleica for Ions of the Energy Range 5-270 Kev/charge on Ampte Irm. *IEEE Trans. Geosci. Remote Sensing* GE-23, 274–279. doi:10.1109/TGRS.1985.289527

Moore, T. E., Peterson, W. K., Russell, C. T., Chandler, M. O., Collier, M. R., Collin, H. L., et al. (1999). Ionospheric Mass Ejection in Response to a CME. *Geophys. Res. Lett.* 26, 2339–2342. doi:10.1029/1999gl900456

Mukai, T., Hirahara, M., Machida, S., Saito, Y., Terasawa, T., and Nishida, A. (1994). Geotail Observation of Cold Ion Streams in the Medium Distance Magnetotail Lobe in the Course of a Substorm. *Geophys. Res. Lett.* 21, 1023–1026. doi:10.1029/93gl02424

Nauk, V. I., and Doklady, A. (1961). Nitrogen Ions in the Upper Atmosphere and the Ionization of the Region at Night. *Dokl. Akad. Nauk SSSR* 137:5 (1961), 1102–1105.

Nishida, A. (1994). The Geotail mission. *Geophys. Res. Lett.* 21, 2871–2873. doi:10.1029/94GL01223

Nosé, M., Taguchi, S., Hosokawa, K., Christon, S. P., McEntire, R. W., Moore, T. E., et al. (2005). Overwhelming O+ Contribution to the Plasma Sheet Energy Density during the October 2003 Superstorm: Geotail/EPIC and IMAGE/LENA Observations. *J. Geophys. Res. Space Phys.* 110, 1.

Peterson, W. K., Abe, T., Fukunishi, H., Greffen, M. J., Hayakawa, H., Kasahara, Y., et al. (1994). On the Sources of Energization of Molecular Ions at Ionospheric Altitudes. *J. Geophys. Res.* 99, 23257–23274. doi:10.1029/94JA01738

Poppe, A. R., Fillingim, M. O., Halekas, J. S., Raeder, J., and Angelopoulos, V. (2016). Artemis Observations of Terrestrial Ionospheric Molecular Ion Outflow at the Moon. *Geophys. Res. Lett.* 43, 6749–6758. doi:10.1002/2016GL069715

Richards, P. G., and Voglozin, D. (2011). Reexamination of Ionospheric Photochemistry. *J. Geophys. Res. Space Phys.* 116, 47. doi:10.1029/2011JA016613

Ridley, A. J., Deng, Y., and Tóth, G. (2006). The Global Ionosphere-Thermosphere Model. *J. Atmos. Solar-Terrestrial Phys.* 68, 839–864. doi:10.1016/j.jastp.2006.01.008

Schunk, R., and Nagy, A. (2009). *Ionospheres*. second edn. Cambridge University Press. Cambridge Books Online.

Schunk, R. W., and Raitt, W. J. (1980). Atomic Nitrogen and Oxygen Ions in the Daytime High-Latitude F Region. *J. Geophys. Res.* 85, 1255–1272. doi:10.1029/ja085ia03p01255

Schunk, R. W., Raitt, W. J., and Banks, P. M. (1975). Effect of electric fields on the daytime high-latitude e and f regions. *J. Geophys. Res.* (1896-1977) (80), 3121–3130. doi:10.1029/JA080i022p03121

Schunk, R. W., and Sojka, J. J. (1997). Global Ionosphere-Polar Wind System during Changing Magnetic Activity. *J. Geophys. Res.* 102, 11625–11651. doi:10.1029/97ja00292

Seki, K., Keika, K., Kasahara, S., Yokota, S., Hori, T., Asamura, K., et al. (2019). Statistical Properties of Molecular Ions in the Ring Current Observed by the Arase (Erg) Satellite. *Geophys. Res. Lett.* 46, 8643–8651. doi:10.1029/2019gl084163

Seki, K., Terasawa, T., Hirahara, M., and Mukai, T. (1998). Quantification of Tailward Cold O+beams in the Lobe/mantle Regions with Geotail Data: Constraints on Polar O+outflows. *J. Geophys. Res.* 103, 29371–29381. doi:10.1029/98ja02463

Shelley, E. G., Ghielmetti, A. G., Balsiger, H., Black, R. K., Bowles, J. A., Bowman, R. P., et al. (1995). The Toroidal Imaging Mass-Angle Spectrograph (Timas) for the Polar mission. *Space Sci. Rev.* 71, 497–530. doi:10.1007/bf00751339

Shelley, E. G., Johnson, R. G., and Sharp, R. D. (1972). Satellite Observations of Energetic Heavy Ions during a Geomagnetic Storm. *J. Geophys. Res.* 77, 6104–6110. doi:10.1029/JA077i031p06104

Solomon, S. C., Hays, P. B., and Abreu, V. J. (1988). The Auroral 6300 Å Emission: Observations and Modeling. *J. Geophys. Res.* 93, 9867–9882. doi:10.1029/JA093iA09p09867

Spjeldvik, W. N., and Fritz, T. A. (1981). Observations of Ions with Nuclear charge$Z \geqq 9$ in the Inner Magnetosphere. *J. Geophys. Res.* 86, 7749–7754. doi:10.1029/JA086iA09p07749

Takada, M., Seki, K., Ogawa, Y., Keika, K., Kasahara, S., Yokota, S., et al. (2021). Low-altitude Ion Upflow Observed by Eiscat and its Effects on Supply of Molecular Ions in the Ring Current Detected by Arase (Erg). *J. Geophys. Res. Space Phys.* 126, e2020JA028951. doi:10.1029/2020JA028951

Taylor, H. A., Jr. (1971). Observed Solar Geomagnetic Control of the Ionosphere-Implications for Reference Ionospheres. *Space Res.* 12, 1275–1290.

Taylor, H. A., Brinton, H. C., Pharo, M. W., and Rahman, N. K. (1968). Thermal Ions in the Exosphere; Evidence of Solar and Geomagnetic Control. *J. Geophys. Res.* 73, 5521–5533. doi:10.1029/ja073i017p05521

Taylor, H. A., Grebowsky, J. M., and Chen, A. J. (1975). Ion Composition Irregularities and Ionosphere-Plasmasphere Coupling: Observations of a High Latitude Ion Trough. *J. Atmos. Terrestrial Phys.* 37, 613–623. doi:10.1016/0021-9169(75)90056-2

Taylor, H. A. (1974). High Latitude Minor Ion Enhancements: A Clue for Studies of Magnetosphere-Atmosphere Coupling. *J. Atmos. Terrestrial Phys.* 36, 1815–1823. doi:10.1016/0021-9169(74)90168-8

Taylor, H. A., Jr. (1973). Parametric Description of Thermospheric Ion Composition Results. *J. Geophys. Res.* 78, 315–319. doi:10.1029/JA078i001p00315

Torr, D. G., and Orsini, N. (1978). The Effect of N2+recombination on the Aeronomic Determination of the Charge Exchange Rate Coefficient of O+(^{2}D) with N2d) with N2. *Geophys. Res. Lett.* 5, 657–659. doi:10.1029/GL005i008p00657

Tsuruda, K., and Oya, H. (1991). Introduction to the Exos-D (Akebono) Project. *Geophys. Res. Lett.* 18, 293–295. doi:10.1029/91GL00039

Whalen, B. A., Burrows, J. R., Yau, A. W., Budzinski, E. E., Pilon, A. M., Iwamoto, I., et al. (1990). The Suprathermal Ion Mass Spectrometer(SMS) Onboard the Agebono (EXOS-D) Satellite. *J. Geomagn. Geoelec* 42, 511–536. doi:10.5636/jgg.42.511

Williams, D. J., Lui, A. T. Y., McEntire, R. W., Angelopoulos, V., Jacquey, C., Christon, S. P., et al. (1994). Magnetopause Encounters in the Magnetotail at Distances of ~80 Re 80 Re. *Geophys. Res. Lett.* 21, 3007–3010. doi:10.1029/94gl01298

Wilson, G. R., and Craven, P. (1999). Molecular Ion Upflow in the Cleft Ion fountain - Wilson - 1999-Journal of Geophysical Research: Space Physics - Wiley Online Library. *J. Geophys. Res.* 104, 4437–4446. doi:10.1029/1998JA900070

Winglee, R. M., Chua, D., Brittnacher, M., Parks, G. K., and Lu, G. (2002). Global Impact of Ionospheric Outflows on the Dynamics of the Magnetosphere and Cross-Polar Cap Potential. *J. Geophys. Res.* 107, 1237. doi:10.1029/2001JA000214

Yamauchi, M. (2019). Terrestrial Ion Escape and Relevant Circulation in Space. *Ann. Geophys.* 37, 1197–1222. doi:10.5194/angeo-37-1197-2019

Yau, A. W., Abe, T., and Peterson, W. K. (2007). The Polar Wind: Recent Observations. *J. Atmos. Solar-Terrestrial Phys.* 69, 1936–1983. doi:10.1016/j.jastp.2007.08.010

Yau, A. W., and Howarth, A. (2016). Imaging thermal Plasma Mass and Velocity Analyzer. *J. Geophys. Res. Space Phys.* 121, 7326–7333. doi:10.1002/2016JA022699

Yau, A. W., James, H. G., and Liu, W. (2006). The canadian Enhanced Polar Outflow Probe (E-pop) mission in ilwsMagnetospheric Dynamics and the International Living with a star Program. *Adv. Space Res.* 38, 1870–1877. doi:10.1016/j.asr.2005.01.058

Yau, A. W., Whalen, B. A., Goodenough, C., Sagawa, E., and Mukai, T. (1993). EXOS D (Akebono) Observations of Molecular NO(+) and N2(+) Upflowing Ions in the High-Altitude Auroral Ionosphere. *J. Geophys. Res.* 98, 11205–11224. doi:10.1029/92ja02019

Yau, A. W., Whalen, B. A., and Sagawa, E. (1991). Minor Ion Composition in the Polar Ionosphere. *Geophys. Res. Lett.* 18, 345–348. doi:10.1029/91gl00034

Yokota, S., Kasahara, S., Mitani, T., Asamura, K., Hirahara, M., Takashima, T., et al. (2017). Medium-energy Particle Experiments-Ion Mass Analyzer (MEP-I) Onboard ERG (Arase). *Earth Planets Space* 69, 69. doi:10.1186/s40623-017-0754-8

Zettergren, M., Semeter, J., Burnett, B., Oliver, W., Heinselman, C., Blelly, P.-L., et al. (2010). Dynamic Variability in F-Region Ionospheric Composition at Auroral Arc Boundaries. *Ann. Geophys.* 28, 651–664. doi:10.5194/angeo-28-651-2010

Zettergren, M., Semeter, J., Heinselman, C., and Diaz, M. (2011). Incoherent Scatter Radar Estimation of F Region Ionospheric Composition during Frictional Heating Events. *J. Geophys. Res. Space Phys.* 116, 1. doi:10.1029/2010JA016035

Conflict of Interest: The authors declare that the research was conducted in the absence of any commercial or financial relationships that could be construed as a potential conflict of interest.

Publisher's Note: All claims expressed in this article are solely those of the authors and do not necessarily represent those of their affiliated organizations, or those of the publisher, the editors, and the reviewers. Any product that may be evaluated in this article, or claim that may be made by its manufacturer, is not guaranteed or endorsed by the publisher.